Quantitative Indoor-Outdoor Evaluation Framework For ERI Windshield Tags In Intelligent Transportation Systems

Xiaowei Zhu¹, Yang Bao¹, Houlong Qian¹, Lingling Kang¹ Shanghai IC Technology & Industry Promotion Center, China

Abstract:

Existing Electronic Registration Identification (ERI) standards specify installation and basic readability but lack a quantitative, cross-scenario benchmark. We propose a reproducible indoor—outdoor framework with unified geometry and metrics. In a full anechoic chamber, ultra-high-frequency (UHF) ERI windshield tags were tested on ten windshields (920–925 MHz; 0° , 30° , 60° , 90°), reporting activation thresholds, and a Friis-based relative forward-link distance (R_{theory}). Outdoor validation on 22 vehicles examined coated/tinted glass, RF-transparent microwave windows, tag placement, temperature, and nearby on-glass devices. Results show: after channel equalization, oblique incidence (60° – 90°) changed activation thresholds by 1.6–5.9 dB (n=10, median = 2.0 dB, measurement uncertainty ≤ 0.6 dB) relative to 0° ; metallized coatings, heating wires, and thick laminates can render center placement unreadable, whereas microwave windows restored readability in the tested cases; elevated tag temperature degrades response; and electronic toll collection (ETC) units or dashcams are negligible unless they occlude the tag. A closed-section drive (10–60 km/h) observed an $\approx 86\%$ drop in read counts with speed, consistent with an engineering recommendation of ~ 3 –6 dB additional link margin and multi-antenna coverage. The framework provides quantitative guidance for installation and reader siting/power planning and enables consistent comparison across materials and environments.

Key Word: Electronic Registration Identification (ERI); RFID; intelligent transportation systems; windshield materials; forward-link sensitivity.

Date of Submission: 08-11-2025

Date of Acceptance: 18-11-2025

I. Introduction

Radio-frequency identification (RFID) is a core identification technology in intelligent transportation and the Internet of Things, valued for non-contact operation, high concurrency, and low cost¹. It is deployed in industrial logistics, supply chains, and automatic vehicle identification (e.g., ISO/IEC 18000-63 air interface; ISO/IEC 18047-6 conformance)². Within this ecosystem, passive ultra-high-frequency (UHF) tags underpin vehicle Electronic Registration Identification (ERI), enabling in-motion recognition by roadside units³.

International studies have examined ERI performance in specific contexts—such as European high-speed tolling and North American deployments/interference—yet most remain single-scenario and do not systematically assess environmental or material factors ^{4,5}. The Chinese standard GB/T 35790.1–2017 specifies installation and basic readability but not quantitative performance ("how well it can be read"), leaving a gap for cross-scenario metrics.

We address this gap with an integrated indoor-outdoor evaluation framework for vehicle ERI. Indoor tests in a full anechoic chamber quantify tag behavior on different windshield materials—including microwave windows and metallic coatings—at controlled geometries; outdoor static tests on real vehicles validate material and placement effects under practical conditions. Together they establish a unified metric system that links laboratory material adaptability with multi-condition road outcomes, informing ERI product selection, installation best practices, and deployment; a supplemental closed-section dynamic check relates static metrics to driving conditions.

To meet engineering needs, the test system offers: frequency coverage of 920–925 MHz⁶; 0.1 dB power steps with combined standard uncertainty $P_{th} \le 0.6$ dB and induced R_{theory} uncertainty $\approx \pm (6-8)\%$ (e.g., ± 0.3 m at R \approx 4.5 via Eq. (1))⁷; per-condition acquisition ≤ 1 s enabling efficient multi-angle scans⁸; sensitivity resolution below -10 dBm⁹; and environmental compatibility up to ≥ 60 °C and across common windshield structures¹⁰. Unlike prior single-scenario or proprietary platforms, our method provides a standardized, cross-scenario consistency evaluation tailored to ERI tags, together with a cross-environment alignment model and unified performance criteria¹¹, and is extensible to other RFID-based transportation identification applications¹².

DOI: 10.9790/2834-2006012335 www.iosrjournals.org 23 | Page

II. Materials And Methods

Electronic Registration Identification (ERI) based on passive UHF RFID exhibits in-use performance that depends on the tag and its mounting medium, as well as the reader–tag geometry¹³. The experimental design focuses on the tag–windshield combination rather than network or controller aspects of the reader infrastructure¹⁴. The workflow comprises (i) indoor measurements in a full anechoic chamber to quantify effects of windshield material and installation, followed by (ii) outdoor static tests on production vehicles under practical conditions, using an aligned frequency band and incidence angles to enable direct comparison and mapping of results¹⁵. A supplemental closed-section dynamic experiment (10–60 km/h) adopts identical RF settings and geometry and records read counts as an observational endpoint. The evaluated metrics include the forward-link sensitivity threshold P_{th} , a Friis-based relative theoretical working distance R_{theory} , and the optimal operating frequency range¹⁶.

Test Model and Metrics

A reader–tag geometric model representative of road scenarios is considered (Figure 1). The reader antenna is mounted on roadside infrastructure (e.g., gantry or side mast) with a downward orientation toward traffic; the ERI tag is attached to the interior surface of the front windshield. During passage through the coverage zone, the incidence angle θ between the antenna boresight and the tag normal varies from approximately 90° at entry to 0° beneath the antenna and then back toward 90°. Four representative angles are used: θ =0°, 30°, 60°, and 90°.

Symbols and definitions.

f: operating frequency (Hz); test band 920–925 MHz, $\lambda = c/f$.

 P_{EIRP} : equivalent isotropic radiated power of the reader (W); unless stated otherwise, a reference of 35 dBm is applied.

 P_{th} : minimum received power at the tag input (W or dBm) for first response under fixed geometry/angle/frequency; when given in dBm, $P[mW]=10^{P[dBm]/10}$.

Metrics: forward-link sensitivity threshold P_{th} , relative theoretical working distance R_{theory} , and optimal operating band.

Relative forward-link distance.

Under free-space far-field conditions with matched linear polarization and without explicit modeling of multipath or vehicle scattering, the activation threshold is mapped to a relative distance via the Friis relation ¹⁷:

$$R = \frac{\lambda}{4\pi} \sqrt{\frac{P_{\text{EIRP}}}{P_{th}}} \tag{1}$$

Equation (1) represents the reader \rightarrow tag power-up condition. Actual decodable range also depends on receiver sensitivity and protocol timing, which are not modeled here. Accordingly, R_{theory} is interpreted as a relative comparison metric normalized to a reference P_{EIRP} =35 dBm, not as an absolute field read range, and this normalization is independent of the conducted output ceiling used during measurements.

Assumptions and boundaries (condensed).

Calibration/equalization. Cable and switch losses are calibrated per angle port; residual inter-port mismatch lies within ± 0.3 –0.5 dB. Angle-dependent antenna response is measured at 1 m and used to amplitude-equalize the four ports; remaining pattern mismatch (≤ 0.5 dB) is included in uncertainty.

Region of operation. With windshield dimension D and $\lambda \approx 0.33$ m, the 1 m setup is within the radiating near-field/transition region; Eq. (1) is therefore used as a relative indicator, and near-field effects are treated as common-mode within the reported uncertainty.

Polarization/propagation. Reader and tag are linearly polarized. Multipath, passenger shadowing, and polarization mismatch are not modeled in Eq. (1).

Scope. Eq. (1) addresses forward-link activation; receiver-side factors (e.g., detection thresholds, protocol timing) are outside the model.

Measurement ceiling. The instrument output power was swept up to $P_{out,max}$ =29 dBm; the instantaneous EIRP followed $P_{EIRP} = P_{out} + G_{ant} - L_{cable}$ (dB). "NA" indicates no tag response up to $P_{out,max}$ (i.e., the true P_{th} exceeds the measurable range under our setup).

Normalization reference. For cross-condition comparison in Eq. (1), R_{theory} is normalized to a reference P_{EIRP} =35 dBm; this serves as a common yardstick and does not reflect the conducted power used during data acquisition.

24 | Page

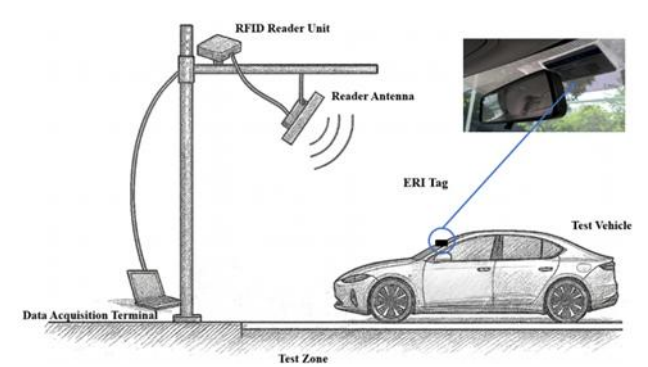


Figure 1. Reader–tag geometry in a road scenario with four incidence angles $(0^{\circ}-90^{\circ})$ along the vehicle trajectory.

Indoor Windshield Material Adaptability Tests Environment and equipment.

Indoor measurements were performed in a full anechoic chamber. Ambient pressure was 86–106 kPa and temperature 23 ± 5 °C. Chamber RF shielding effectiveness measured 90 dB over 800 MHz–1 GHz. The setup employed a Voyantic Tagformance Pro with a four-port switch and linearly polarized antennas. A 920–925 MHz sweep with 1 MHz resolution was used. Equipment warm-up followed manufacturer specifications. Reader power step was 0.1 dB; considering output accuracy, cable/switch drift, pattern equalization, and placement tolerance, the combined standard uncertainty of P_{th} was \leq 0.6 dB, propagated to R_{theory} via (1). "NA" indicates no tag response at 29 dBm instrument output.

Geometry and installation.

Four identical linearly polarized patch antennas were placed on a common arc with 30° spacing; boresights intersected at the arc center, realizing θ =0°, 30°, 60°, and 90°. Each antenna was positioned 1 m from the windshield center. Detached front windshields were mounted with the long edge parallel to antenna polarization. The ERI tag was first affixed at the geometric center on the interior surface. When the center position produced no response at the available power, retesting was conducted at the RF-transparent "microwave window" specified by GB/T 35790.1–2017 to separate material and placement effects¹⁸. Figure 2 illustrates the layout.

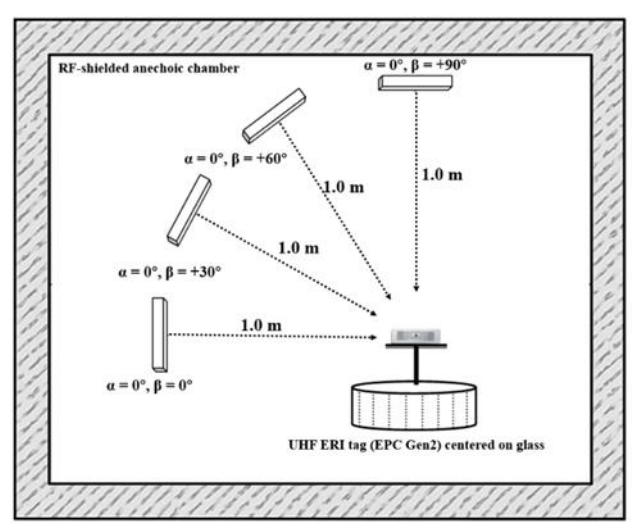


Figure 2. Indoor test setup showing the four linearly polarized reader antennas arranged at incidence angles of 0°, 30°, 60°, and 90° relative to the test windshield. The ERI tag is mounted on the interior side of the windshield (at the center or at the designated microwave window position if the center yields no read).

Procedure and data recording.

Ten front windshields representative of common vehicles were examined, covering coated or wire-heated glass, acoustic/HUD laminated constructions, embedded-antenna glass, and plain truck/bus glass. For each windshield, frequency sweeps were performed at θ =0°, 30°, 60°, and 90°. At each frequency, the Tagformance system determined the lowest transmit power eliciting a tag response; this value was recorded as P_{th} . The relative theoretical working distance R_{theory} was computed for P_{EIRP} =35 dBm using (1). The optimal operating band per

angle was defined as the frequency set with P_{th} within +1 dB of the minimum over 920–925 MHz (equivalently $R_{theory} \ge 0.89 R_{max}$). When both center and window placements were tested, both datasets were retained for material-versus-placement comparison¹⁹.

Data use and criteria.

Indoor results quantified the effects of "windshield material \times incidence angle" on the forward link and provided baselines for outdoor tests. As an engineering target under the tested geometry, a threshold sensitivity \leq -10 dBm at θ =0° corresponds to $R_{theory}\geq$ 4.5 m at P_{EIRP} =35 dBm. For samples unreadable at the center but readable at the microwave window, attenuation is attributed to windshield structure; placement within the specified window per GB/T 35790.1–2017 is required for compliant installation²⁰.

Outdoor On-Vehicle Tests

Outdoor experiments were performed on level open ground with at least 3 m clearance from large metallic structures to represent an unobstructed roadside environment²¹. A height-adjustable rig positioned four linearly polarized reader antennas at θ =0°, 30°, 60°, and 90° around a central point²². For each test, the vehicle's ERI tag was placed at the center of this antenna arc to replicate the indoor geometry (Figure 3). A Tagformance RFID performance tester with the antennas and control software used in the indoor setup was deployed outdoors to maintain measurement comparability²³. For each vehicle, records included the presence of aftermarket windshield tint film, a factory-designated RF-transparent "microwave window," and nearby on-glass devices (e.g., ETC units, dashcams) located at or near the tag area²⁴. Environmental variables (ambient temperature, atmospheric pressure, solar illumination) were logged during testing²⁵.

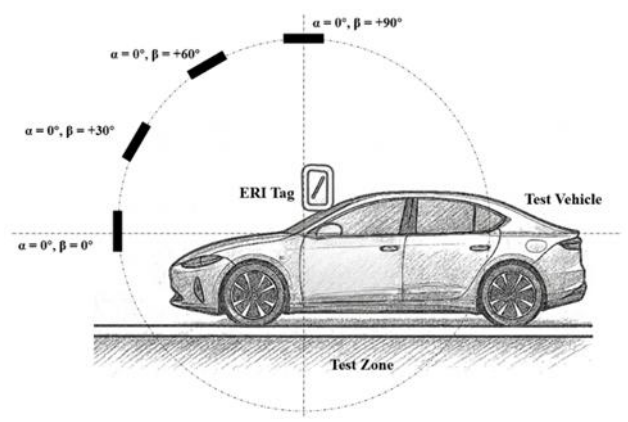


Figure 3. Outdoor test platform setup. The four reader antennas are positioned on a frame such that they form the same angular geometry as used in the indoor test $(0^{\circ}, 30^{\circ}, 60^{\circ}, 90^{\circ})$ around the tag). The height of the antenna rig is adjusted to align with the position of the tag on the vehicle's windshield. A car is parked at the test position for static measurement.

Each vehicle was positioned at the designated location within the antenna arc. The same ERI tag model as used indoors was installed per the guideline (upper-center or upper-corner, or within the factory microwave window when available). Before acquisition, the equipment was warmed up and calibrated; cable/switch losses and per-port antenna responses were measured and amplitude-equalized.

Table 1. Windshield samples used in indoor tests (with key characteristics).

| ID | Windshield Description | Key Features (concise) | | | | | |
|-----|-----------------------------------|---|--|--|--|--|--|
| #01 | 2013 Audi A6L front windshield | Coated; rain/night sensors; center unreadable | | | | | |
| #02 | Land Rover Discovery 3 windshield | Heated (tungsten-wire); rain sensor | | | | | |
| #03 | 2012 BMW 3-Series windshield | Rain sensor; HUD combiner; acoustic laminate | | | | | |
| #04 | Land Rover Range Rover windshield | Metallic coating; heating wires; no sensor cut-out; center unreadable | | | | | |
| #05 | 2011 Ford Explorer windshield | Acoustic film laminate; no special sensors | | | | | |
| #06 | Geely King Kong windshield | Embedded radio antenna | | | | | |
| #07 | Ford Explorer | Dual sensor mounts (rain/light) | | | | | |
| #08 | Mercedes-Benz C-Class windshield | Dual sensor module (rain/light) | | | | | |
| #09 | Renault truck front windshield | Standard glass | | | | | |
| #10 | Nissan mid-size bus windshield | Standard large glass | | | | | |

Note: "Center reading failed; tested at window" indicates the tag could not be read at the windshield's center position for that sample, so the tag was moved to the prescribed microwave window area and retested, as per standard installation practice.

For each incidence angle (0°, 30°, 60°, 90°), a sweep over 920–925 MHz was collected by selecting the corresponding antenna port or rotating the rig. To ensure repeatability, each angle×frequency condition was measured five times (n = 5) in immediate succession, and reported results (Tables 2–3) are means from n = 5 repeats; typical standard deviations are within ± 0.3 dB. The extracted metrics were the forward-link sensitivity threshold P_{th} , the Friis-based relative theoretical working distance R_{theory} (normalized to the reference EIRP), and the optimal operating-frequency range²⁶. For vehicles with tinted windshields and/or a factory microwave window, measurements were taken at both placements (tinted area and window). Seasonal sessions (winter and summer) allowed assessment of temperature dependence.

The fleet comprised 22 vehicles: 16 sedans, 4 SUVs, and 2 MPVs (7-seaters), including fuel-powered and hybrid/electric models. Table 4 summarizes model information and the presence of windshield tint and onboard ETC devices.

Table 2. Tag sensitivity (threshold power in dBm) at different antenna incidence angles (selected samples, single-direction test)

| single direction test). | | | | | | |
|-------------------------|------------|----------|-----------|-----------|-----------|--|
| Windshield Sample | Freq (MHz) | 0° (dBm) | 30° (dBm) | 60° (dBm) | 90° (dBm) | |
| #0 <i>C</i> (:tht) | 920 | -6.0 | -8.6 | -9.5 | -11.9 | |
| #06 (with antenna) | 925 | -6.3 | -7.8 | -9.4 | -11.5 | |
| #00 (dood oom) | 920 | -14.8 | -15.5 | -15.9 | -16.0 | |
| #08 (dual sensors) | 925 | -15.1 | -15.8 | -16.2 | -16.2 | |
| #10 (hara alasa) | 920 | -14.7 | -15.7 | -16.1 | -16.3 | |
| #10 (bus glass) | 925 | -14.8 | -15.9 | -16.2 | -16.4 | |

Note: Values are means of n = 5 consecutive repeats per angle/frequency/placement; typical SD \leq 0.3 dB. "NA" indicates no tag response up to the instrument output ceiling (29 dBm)

Table 3. Tag sensitivity on different windshield materials (threshold power in dBm at 920/925 MHz for 0°-90° angles)

| angles). | | | | | | |
|----------|------------|----------|-----------|-----------|-----------|--|
| ID | Freq (MHz) | 0° (dBm) | 30° (dBm) | 60° (dBm) | 90° (dBm) | |
| //01 | 920 | NA* | NA | NA | NA | |
| #01 | 925 | NA | NA | NA | NA | |
| #02 | 920 | -10.0 | -10.6 | -10.3 | -12.2 | |
| #02 | 925 | -9.9 | -10.9 | -10.8 | -12.7 | |
| #03 | 920 | -14.1 | -14.0 | -14.5 | -14.7 | |
| 1103 | 925 | -14.2 | -14.4 | -14.9 | -15.2 | |
| #04 | 920 | NA | NA | NA | NA | |
| #04 | 925 | NA | NA | NA | NA | |
| #05 | 920 | -14.1 | -15.4 | -15.0 | -15.4 | |
| #03 | 925 | -14.7 | -15.8 | -15.2 | -15.7 | |
| #06 | 920 | -6.0 | -8.6 | -9.5 | -11.9 | |
| 1100 | 925 | -6.3 | -7.8 | -9.4 | -11.5 | |
| #07 | 920 | -12.1 | -14.2 | -14.0 | -15.2 | |
| #07 | 925 | -12.8 | -14.5 | -14.5 | -15.5 | |
| #08 | 920 | -14.8 | -15.5 | -15.9 | -16.0 | |
| #08 | 925 | -15.1 | -15.8 | -16.2 | -16.2 | |
| #09 | 920 | -14.9 | -15.7 | -15.9 | -15.9 | |
| #03 | 925 | -15.1 | -16.0 | -16.2 | -16.2 | |
| #10 | 920 | -14.7 | -15.7 | -16.1 | -16.3 | |
| #10 | 925 | -14.8 | -15.9 | -16.2 | -16.4 | |

^{*} Not available (NA) entries indicate no tag response at maximum reader power (29 dBm at the instrument output) for that configuration. Samples #01 and #04 could not be read at the center position; their performance was recovered when the tag was moved to the prescribed microwave window area (not shown in the table).

Table 4. Summary of vehicles used in outdoor tests and their characteristics.

| ID | Manufacturer | Model | Type | Tinted | ETC |
|----|--------------|------------|------|--------|-----|
| 1 | Beijing Benz | C200L | Fuel | Yes | No |
| 2 | BMW | 320i | Fuel | Yes | Yes |
| 3 | BMW | 530Le | PHEV | Yes | No |
| 4 | SAIC GM | Excelle GT | Fuel | Yes | No |
| 5 | SAIC GM | ATS-L | Fuel | Yes | No |
| 6 | Dongfeng | Citroën C5 | Fuel | Yes | Yes |
| 7 | Infiniti | G25 | Fuel | Yes | No |
| 8 | Jaguar | XFL 2.0T | Fuel | Yes | No |

| 9 | Volkswagen | Superb TSI 280 | Fuel | Yes | Yes |
|----|--------------|----------------|------|-----|-----|
| 10 | Volkswagen | Octavia | Fuel | Yes | No |
| 11 | Honda | Civic | Fuel | Yes | No |
| 12 | Mazda | Mazda3 Axela | Fuel | Yes | No |
| 13 | SAIC Motor | MG6 | Fuel | No | No |
| 14 | Lexus | Lexus ES200 | Fuel | Yes | Yes |
| 15 | BYD Auto | BYD Qin | PHEV | No | No |
| 16 | Roewe | Roewe 550 | PHEV | Yes | No |
| 17 | Beijing Benz | GLC260L | PHEV | Yes | No |
| 18 | Subaru | Forester 2.0 | Fuel | Yes | No |
| 19 | Yueda Kia | Sportage R | Fuel | Yes | No |
| 20 | SAIC GM | GL8 | Fuel | Yes | Yes |
| 21 | SAIC GM | Envision 28T | Fuel | Yes | No |
| 22 | SAIC GM | GL8 25S | Fuel | Yes | Yes |

III. Results

Indoor Test Results (Windshield Material Adaptability)

The results from the indoor anechoic chamber tests on the 10 windshield samples were first analyzed. These tests quantified how the tag's performance varied with incidence angle and windshield material.

Effect of Antenna Angle on Tag Performance

After channel equalization, comparing θ =60°-90° with θ =0° yielded sample-dependent differences of 1.6–5.9 dB in P_{th} (median ≈ 2 dB). These variations, although modest in magnitude (typically within 1–6 dB), consistently exceeded the measurement uncertainty (\leq 0.6 dB), indicating a reproducible but limited effect that is mainly of engineering relevance. Examples include windshield #06: P_{th} from -6.03 dBm (0°) to -11.94 dBm (90°), and windshield #10: from -14.75 dBm (0°) to -16.39 dBm (90°) (Table 2). These variations reflect tag—windshield—angle coupling rather than antenna pattern effects. Oblique incidence (60°-90°) generally produced lower thresholds than broadside, consistent with radiation-pattern and polarization interactions through glass. Outdoor observations showed a similar trend, with increased read likelihood at oblique incidence and within microwave-window placement²⁷.

Effect of Windshield Material on Performance

Windshield construction influenced tag sensitivity. Plain automotive glass yielded lower thresholds, whereas metallic coatings, embedded wires, and functional laminates increased P_{th} . With normal incidence, #06 (embedded antenna, otherwise standard) exhibited about -6 dBm, #02 (tungsten-wire heating, sensor region) about -10 dBm, and #09/#10 (truck/bus, plain glass) about -15 dBm (Table 3). #01 and #04 (metallized/heated) were unreadable at the center at the instrument's 29 dBm output (NA). The material dependence aligns with RF shielding/scattering by metallic layers or wires and with additional loss/reflection in laminated stacks, particularly where interlayers include HUD combiners or IR-reflective films.

Role of the Microwave Window

For #01 and #04, relocating the tag to the GB/T 35790.1–2017 microwave-window region produced responses at 0°–90°. The window—an untreated area near the rearview-mirror region—provides reduced attenuation, and relocation restored readability relative to the metallized central area. These results indicate that placement within RF-transparent regions is a decisive factor for coated or heated windshields.

Summary

Indoor anechoic measurements quantified the effects of incidence angle and windshield composition on ERI tag activation.

Incidence angle. Activation thresholds at $60^{\circ}-90^{\circ}$ were lower than at $0^{\circ}-30^{\circ}$. Across the tested samples, differences were 0.6-5.9 dB (median ≈ 2 dB), translating via Eq. (1) to $\approx 7-97\%$ change in R_{theory} (median $\approx 26\%$); most samples clustered around $\sim 10-40\%$, and in the most extreme case the implied change approached a factor of two.

Characterization at multiple angles supports link-margin planning across approach geometries.

Windshield material. Uncoated automotive glass yielded lower thresholds. IR-blocking metallic films, embedded heating wires, and acoustic/HUD laminates increased thresholds by several dB. In metallized cases, center placement produced no response under the available transmit power, whereas placement within the RF-transparent window enabled reading.

Microwave window. Relocation to the manufacturer-designated RF-transparent area restored readability to levels comparable to uncoated glass for windshields that otherwise impeded UHF transmission. Installation within the specified window area reduces material-induced loss.

Methodology. An effective evaluation sequence is: (i) center placement; (ii) window placement if the center yields no response. Extended testing may include tag rotation or windshield tilt. A representative panel benefits from including laminated, embedded-antenna, wire-heated, and coated glass.

Target criterion. Based on the indoor dataset, a threshold sensitivity of $P_{th} \le -10$ dBm at $\theta = 0^{\circ}$ (normal incidence through glass) is a practical benchmark; under $P_{EIRP} = 35$ dBm, Eq. (1) maps this to $R_{theory} \ge 4.5$ m.

Outdoor Test Results (Real-Vehicle Performance)

Field tests were conducted in two seasons to assess temperature effects: two sessions in January (\approx 4–8 °C; one sunny and one overcast) and one session in June (30–32 °C; sunny). The outdoor measurements replicated the indoor static geometry. Figure 4 illustrates the outdoor static test setup, and Table 4 summarizes the tested vehicles and configurations (e.g., aftermarket windshield tint, presence of ETC devices).





Figure 4. Outdoor static test setup for ERI tag evaluation. (a) Side view of the height-adjustable frame holding four linearly polarized patch antennas; the vehicle is parked at the measurement position and the reader/measurement unit is placed to the side. (b) Front view showing the four antennas arranged to realize incidence angles of 0°, 30°, 60°, and 90° around the tag location on the windshield. Frequency sweeps across 920–925 MHz were performed at each angle under the same static geometry as in the anechoic-chamber tests.

Effect of Temperature (Winter vs Summer, and Heat Exposure)

Ambient temperature and solar loading affected performance. In January, relative theoretical working distance R_{theory} was lower than in June for several vehicles across 920–925 MHz; the Buick Envision 28T (#21) illustrates this trend (Figure 5).

During the June campaign, a heat-soak experiment was performed: after baseline measurements at \sim 30 °C, vehicles were parked under direct sunlight until the tag surface exceeded \sim 60 °C, followed by repeated measurements. For the Infiniti G25 (#7), R_{theory} decreased in the heat-soaked state (Figure 6), consistent with an increased activation threshold attributable to temperature-dependent IC/antenna behavior.

Overall, colder conditions were associated with modest reductions in R_{theory} , whereas elevated tag temperature produced a more pronounced decrease. For deployment, additional link margin and reader autotuning are recommended for high-temperature operation.

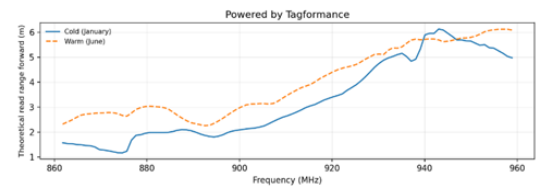


Figure 5. Relative theoretical working distance (R_{theory}) vs. frequency for a Buick Envision 28T (#21) tested in January (cold conditions, dashed curve) and in June (warm conditions, solid curve). The tag's performance was generally better in the warmer test. However, extreme heat caused a decline in performance, as shown in Figure 6.

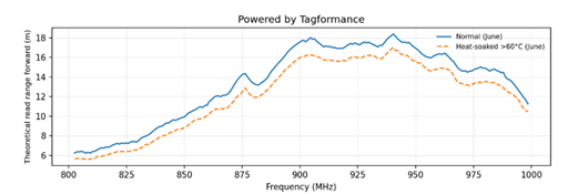


Figure 6. Relative theoretical working distance (R_{theory}) vs. frequency for an Infiniti G25 (#7) in June, comparing normal ambient temperature (solid curve) to after prolonged sun exposure, where the tag's temperature exceeded $\sim 60~^{\circ}\text{C}$ (dashed curve). The relative theoretical working distance dropped at high tag temperature, indicating reduced performance when the tag/vehicle is extremely hot.

Effect of Windshield Tint Film and Microwave Window

Outdoor measurements indicated that aftermarket windshield tint and the use of an RF-transparent "microwave window" were influential variables. Many sedans in the sample had metallic or nano-ceramic films for UV/IR control, which introduce RF attenuation. Vehicles without tint tended to exhibit longer relative theoretical working distance (R_{theory}) than vehicles with tint; for example, the BYD Qin (#15, no tint) exceeded the Mazda3 Axela (#12, with tint) across 920–925 MHz (Figure 7).

In a representative case (Subaru Forester #18 with a metallic film), tag placement on the tinted central region yielded infrequent responses at typical power levels, whereas placement within the factory microwave window (an untinted patch near the rearview mirror) restored readability and R_{theory} (Figures 8–9). For vehicles equipped with metallic or low-emissivity films, locating the tag within a microwave window or other clear area is therefore advisable.

Tint films are heterogeneous. Modern nano-ceramic films may contain less metal and can produce smaller RF loss; however, degradation of R_{theory} was observed for many tinted windshields under the controlled settings used. Readability on tinted regions was sometimes maintained when the reader operated at higher P_{EIRP} or reduced distance, albeit with reduced margin, whereas metallic films occasionally prevented reading until the tag was moved to an RF-transparent area.

Window geometry also affects performance. Very small windows or suboptimal placement can constrain the set of effective orientations. In the tested fleet, factory windows supported static reading at θ =0°, 30°, 60°, and 90°. These observations support standardizing a minimum window size and placement in line with GB/T 35790.1.

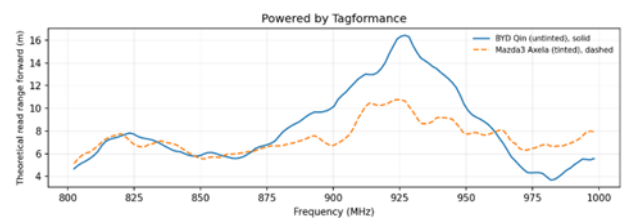


Figure 7. Relative theoretical working distance (R_{theory}) vs. frequency for an untinted windshield (BYD Qin sedan, #15; solid) and a tinted windshield (Mazda3 Axela, #12; dashed). The untinted case shows higher R_{theory} across 920–925 MHz, whereas the tint reduces R_{theory} due to added attenuation.

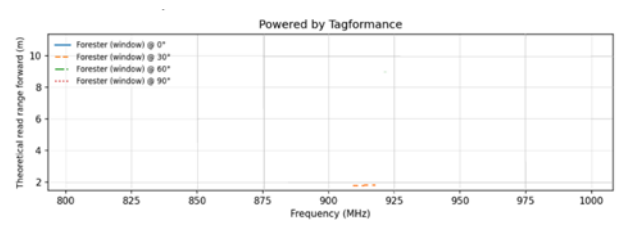


Figure 8. Relative theoretical working distance (R_{theory}) vs. frequency for a Subaru Forester (#18) with the tag installed on a tinted area of the windshield. R_{theory} is very low (barely readable) due to the metallic film's attenuation.

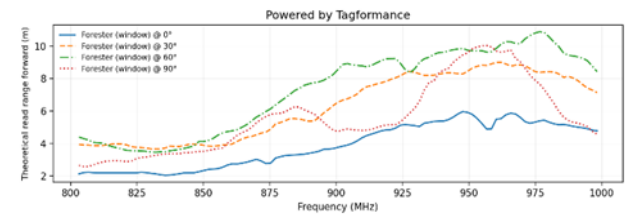


Figure 9. Relative theoretical working distance (R_{theory}) vs. frequency for the Subaru Forester (#18) with the tag installed at the windshield's RF-transparent microwave window. R_{theory} is restored, confirming the window's effectiveness.

Effect of Open Windows (Vehicle Cabin Venting)

This subsection evaluates whether opening side windows or a sunroof influences reading of a windshield-mounted ERI tag. Comparative measurements were performed on several vehicles (including a

Subaru Forester) under a static geometry, using identical RF settings, with three conditions: all windows closed, one side window open, and sunroof open.

The relative theoretical working-distance curves and threshold values under the three conditions were within the measurement repeatability of the setup and showed no systematic shift (Figures 10–12). The data are consistent with a reader–tag coupling dominated by the line-of-sight path through the windshield under the tested configuration; additional paths introduced by open apertures did not produce measurable changes in the link budget.

Under comparable static tests and geometry, window state is therefore not treated as a control variable for ERI performance assessment.

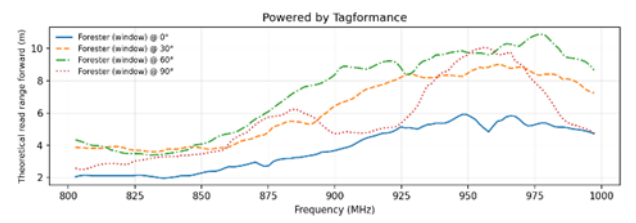


Figure 10. Relative theoretical working distance (R_{theory}) vs. frequency for the Subaru Forester (#18) with all doors and windows closed (baseline).

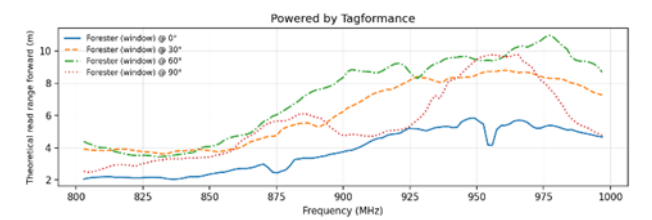


Figure 11. Relative theoretical working distance (R_{theory}) vs. frequency for the Subaru Forester (#18) with a side window open; performance is essentially unchanged compared with Figure 10.

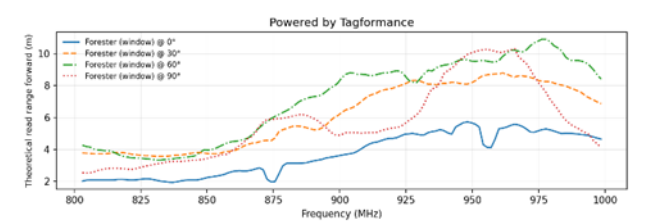


Figure 12. Relative theoretical working distance (R_{theory}) vs. frequency for the Subaru Forester (#18) with the sunroof open; performance is similar to the closed condition.

Impact of On-Board Devices (ETC Units, Dashcams)

On-glass devices near the interior windshield—dash cameras, rain/light sensor housings, and 5.8-GHz Electronic Toll Collection (ETC) transponders—can introduce geometric shadowing of the ERI tag. In the examined fleet, dash cameras were present on more than half of vehicles (commonly behind or below the rearview mirror), and ETC devices on approximately one-third (often near the upper center). Device—tag separation was documented for all vehicles.

Under the static geometry and frequency band of this study, configurations without physical overlap between device and tag did not show measurable degradation of ERI response within the measurement sensitivity. Small lateral offsets of a few centimeters used to avoid overlap produced performance comparable to unadjusted placements. In contrast, placing the tag directly behind an ETC unit is expected to reduce successful reads due to shadowing. These observations align with the frequency separation between UHF ERI links and 5.8-GHz ETC, which limits in-band coupling. Installation practice is therefore recommended to maintain clear line-of-sight and a minimum spacing from on-glass devices to mitigate occlusion.

Effect of Vehicle Type and Windshield Geometry

Across sedans, SUVs, and minivans, tag readability in SUVs and larger vehicles was non-inferior and was often higher than in sedans. Three geometric factors are salient: (i) a more upright windshield improves alignment to overhead beams; (ii) a higher tag mounting height reduces vertical separation from the reader

antenna; and (iii) a larger frontal area increases effective reflective aperture under the test geometry, with multipath controlled. For illustration, the Buick GL8 minivan (#20, #22) and the Mercedes GLC SUV (#17) produced R_{theory} values at certain angles on the upper side of the sample distribution. These observations indicate feasibility across vehicle categories when antenna height and downtilt are configured to cover the sedan–SUV vertical span.

Summary

Outdoor vehicle tests were consistent with indoor findings and added deployment-oriented observations:

Windshield films/materials. Metallic or metallized tint films were associated with reduced read performance unless tags were placed on untreated glass. For vehicles with aftermarket films, a film-free patch (microwave window) or an RF-tolerant film type may be required to maintain margin.

Microwave window. Installation within the manufacturer-designated RF-transparent window (GB/T 35790.1 Appendix A) improved readability, including for vehicles with IR-reflective windshields. The data indicated a marked placement dependence.

Environment (temperature). Elevated tag temperature was associated with degraded response; low ambient temperature showed a smaller reduction. Test protocols benefit from explicit high-temperature trials and environmental logging. Precipitation and heavy dust were not covered and merit separate evaluation.

Vehicle diversity. Model-to-model variation was observed. Under the 35 dBm EIRP reference and with standard placement, vehicle—tag combinations in the sample were readable in static tests. System design should account for less favorable combinations (e.g., metallized glass at high temperature and oblique angles). A diverse vehicle set is useful for characterizing variability across sedans, SUVs, and MPVs, with and without tint films.

On-glass devices. Dashcams and ETC units did not introduce observable UHF interference in the sample; performance degradation is primarily expected when such devices occlude the tag. Maintaining physical clearance is advisable.

Static vs. dynamic. Most measurements were static. A supplemental closed-section test (10–60 km/h; Section 3.3) showed a monotonic decline in read counts with speed. Deployments can allocate \sim 3–6 dB additional link margin and consider multiple antennas or higher EIRP to offset reduced dwell time at higher speeds.

For cross-vehicle comparability, outdoor ERI tests are recommended to place tags in standardized microwave window positions (GB/T 35790.1–2017, Appendix A). For certification or acceptance testing, evaluations in the optimal (window) configuration provide a consistent basis for determining compliance.

Dynamic On-Road Test (Closed Test Section)

To verify the applicability of the outdoor static findings under driving conditions, a dynamic test was conducted on a closed highway test section (Figure 13). One roadside reader antenna was deployed on each side; their installation heights and downtilts matched the prior outdoor static configuration (with small instantaneous incidence-angle variations due to road geometry). The operating band and transmit power were identical to those used previously. The test vehicle traversed the read window in straight-line motion at constant speeds of 10, 20, 30, 40, 50, and 60 km/h; multiple passes were performed at each speed. For each pass, we recorded the number of valid Electronic Product Code (EPC) decodes from the left and right antennas (read counts), used here as the observation for the dynamic scenario. This subsection examines only the effect of vehicle speed on read counts and does not introduce new performance metrics.



Figure 13. Dynamic test setup and field photos on the closed highway test section.

As shown in Figure 14, the read counts decrease monotonically with increasing speed: the left-side count drops from 424 at 10 km/h to 60 at 60 km/h (an 85.8% reduction), and the right-side count from 499 to 66 (an 86.8% reduction). Overall, the trend is approximately linear.

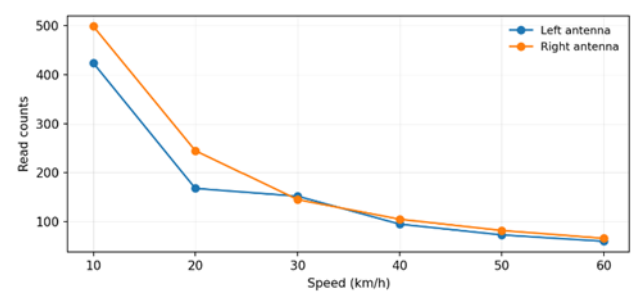


Figure 14. Read-count variation versus vehicle speed for the left and right antennas (trend plot; contains all test data).

IV. Discussion

Indoor and outdoor experiments provided a consistent view of ERI tag behavior in the 920–925 MHz band. Measured relative theoretical working distance (R_{theory}) and sensitivity satisfied traffic identification needs under the tested configurations, with pronounced dependence on windshield construction, incidence angle, and temperature.

Sensitivity varied with incidence. Examples include windshield #06 (threshold from -6.03 dBm at 0° to -11.94 dBm at 90°) and #10 (-14.75 dBm to -16.39 dBm), indicating angle-dependent differences of 1.6-5.9 dB. Outdoor measurements showed higher read reliability at oblique illumination ($60^{\circ}-90^{\circ}$) or when installed within the microwave window. These observations align with polarization coupling and Fresnel transmission effects. Deployment planning benefits from angular coverage via suitable beamwidths or multiple antennas; tag specifications benefit from reporting multi-angle sensitivity rather than broadside only.

Performance differed across glass types. Plain laminated glass yielded lower activation thresholds than coated, wire-embedded, or functionally laminated glass. Sample #02 (heated wires) showed \sim 10 dBm at 0°, whereas #06 (embedded antenna, no metal film) showed \sim 6 dBm, implying a substantial reduction in R_{theory} for unfavorable materials. Metallized windshields (#01, #04) produced no response at center at the instrument's maximum output, while relocation to the microwave window restored readability. Qualification on "difficult" glass (metallized/heated) is recommended; installation within manufacturer-specified windows is recommended where available. Reader EIRP and antenna gain selection needs to reflect material-induced attenuation.

Temperature influenced response. Winter tests (\sim 5 °C) showed lower R_{theory} than moderate summer (\sim 30 °C), and heat-soaked tags (>60 °C) exhibited further degradation. Precipitation effects were not included; particulate contamination and wetting were not evaluated. Engineering practice benefits from additional link margin for thermal excursions, tags with suitable temperature ratings, and operational diversity (e.g., frequency hopping across 920–925 MHz).

Across 22 vehicles, vehicle class exerted a secondary influence; SUVs/vans sometimes achieved longer R_{theory} due to geometry and height. Dashcams and ETC units did not introduce detectable UHF interference; physical shadowing near the tag location remained the primary concern. Installation guidance benefits from maintaining clearance from on-glass devices.

A closed-section test (10–60 km/h) recorded an \sim 86% reduction in read counts with speed. For read-zone length L and speed v, dwell time τ =L/v bounds the number of inventory attempts; maintaining high first-read probability is facilitated by additional link margin (\sim 3–6 dB) and spatial diversity (multi-antenna coverage over 10–15 m).

Recommendations for practice.

- (1) Use RF-transparent microwave windows for coated/filmed windshields; where absent, provide a clear patch at the designated area.
- (2) Avoid metallized or thick laminated regions for tag placement; where unavoidable, consider antenna designs tolerant to dielectric loading and polarization sensitivity.
- (3) Size reader EIRP/antenna gain and coverage angles to accommodate angle/material/temperature-induced sensitivity shifts; employ frequency and spatial diversity.

The test set covered 10 windshield types and 22 vehicles; other constructions (e.g., electrochromic glass) were not included. Dynamic characterization was limited to read-count trends up to 60 km/h without Doppler/fading analysis. A single reader platform and antenna set were used; interactions with other hardware were not assessed. Multi-tag concurrency, precipitation, and urban EMI conditions were not evaluated.

Planned extensions include higher-speed drive-by tests, multi-reader layouts, concurrency and anticollision evaluation, broader environmental conditions, and composite performance indices combining sensitivity and R_{theory} under operational constraints.

V. Conclusions

This paper presented a unified indoor–outdoor evaluation framework for vehicle Electronic Registration Identification (ERI) windshield tags. By coupling full-anechoic adaptability tests with static on-vehicle trials and a supplemental dynamic on-road check (10-60 km/h) under a shared geometry and metric set (0° , 30° , 60° , 90° ; 920-925 MHz), we evaluated 10 windshields and 22 vehicles, measuring activation-sensitivity threshold and relative theoretical working distance.

Methodological and standardization contributions. The study (i) establishes a cross-environment metric system and consistency mapping that aligns laboratory material tests with on-road outcomes; (ii) introduces quantitative performance criteria (sensitivity and relative distance) for like-for-like comparison across materials and geometries; and (iii) provides reproducible procedures and pass/fail recommendations that can support product certification and inform future ERI performance standards. The principal findings and their deployment implications are as follows:

- (1) Windshield materials dominate the link budget. Plain, non-metallic glass provides lower activation thresholds and longer working distance than metallized, wire-heated, or thick laminated glass; in extreme cases, center placement on metallized glass was unreadable at practical EIRP.
- (2) Installation location is decisive; microwave windows restore readability. Positioning the tag in the manufacturer-specified RF-transparent window consistently converted near-unreadable cases into normal operation on coated/filmed windshields. Where no window exists, a small film-free patch is required. Adherence to GB/T 35790.1-2017 is essential.
- (3) Environment matters—plan link margin. Sun-heated tags showed degraded sensitivity and R_{theory} , whereas cold imposed a smaller penalty. A supplemental dynamic on-road test (10–60 km/h) observed decreased read counts with speed; at higher speeds reduced dwell time is expected. Deployments should budget \approx 3–6 dB of link margin (e.g., higher EIRP and/or multiple antennas) for heat and speed.
- (4) Vehicle-class differences are manageable; avoid physical shadowing. SUVs and vans performed on par with or slightly better than sedans. On-glass accessories (ETC units, dashcams) did not interfere unless they physically blocked the tag; maintain several centimeters of clearance.
- (5) Practical implications for transport deployment. The framework provides actionable guidance for roadside reader siting and configuration (antenna height/boresight to cover sedan—SUV span), installation policies (mandatory microwave window placement or film-free patches), and acceptance testing (use the unified metrics as a commissioning checklist). It enables agencies and operators to benchmark ERI products across materials and environments and to make data-driven decisions on reader power, antenna layouts, and maintenance thresholds.

Future work. To serve large-scale ITS deployments, future studies will extend to dynamic drive-by tests across speeds and lanes, multi-tag/urban-RF scenarios, multi-vendor interoperability/anti-collision, and antenna/layout optimization for lane coverage. Developing a composite performance index that combines sensitivity and relative distance under conditions will further support regulatory specification and procurement.

In summary, by linking laboratory adaptability tests with real-vehicle validation through a quantitative, reproducible protocol, this work offers a benchmark for ERI deployment in intelligent transportation systems and a stepping stone toward harmonized performance standards for RFID-based vehicle identification.

References

- [1]. T. M. Fernández-Caramés, "A Bluetooth 5 Opportunistic Edge Computing System For Vehicular Scenarios," Eng. Proc., Vol. 27, 2022, Doi: 10.3390/Ecsa-9-13214.
- [2]. C. L. Baumbauer, D. A. Baumbauer, And A. C. Arias, "The Effect Of Soil Water Content And Crop Canopy On Passive Uhf-Rfid Wireless Links," Comput. Electron. Agric., Vol. 237, 2025, Art. No. 110506, Doi: 10.1016/J.Compag.2025.110506.
- [3]. S. Fu, G. E. Bridges, And B. Kordi, "Rfid Sensor With Integrated Energy Harvesting For Wireless Measurement Of Dc Magnetic Fields," Sensors, Vol. 25, No. 10, 2025, Art. No. 3024, Doi: 10.3390/S25103024.
- [4]. H. Anam, S. M. Abbas, I. B. Collings, Et Al., "Materials-Driven Advancements In Chipless Radio-Frequency Identification And Antenna Technologies," Sensors, Vol. 25, No. 9, 2025, Art. No. 2867, Doi: 10.3390/S25092867.
- [5]. M. Naveed, U. Sadiq, S. Abubakar, N. Muhammad Waqas, A. Ahmed, I. Muhammad Ali, And A. Qammer H., "Iot Enabled Vehicle Recognition System Using Inkjet-Printed Windshield Tag And 5g Cloud Network," Internet Things, Vol. 23, 2023.
- [6]. X. Wang, J. Zhang, S. Mao, Et Al., "A Framework For Locating Multiple Rfid Tags Using Rf Hologram Tensors," Digit. Commun. Netw., Vol. 11, No. 2, Pp. 337–348, 2025, Doi: 10.1016/J.Dcan.2023.12.004.
- [7]. R. Das, T. Das, And A. K. Yadav, "Design And Analysis Of Gain-Enhanced Zim Superstrate-Based Antenna For Rfid Reader Applications," Int. J. Commun. Syst., Vol. 38, No. 7, 2025, Art. No. E70025, Doi: 10.1002/Dac.70025.
- [8]. L. Ang, L. Jiawei, Z. Yan, H. Dianqi, L. Tao, And Z. Yanchao, "Secure Uhf Rfid Authentication With Smart Devices," Ieee Trans. Wireless Commun., Vol. 22, No. 7, Pp. 4520–4533, 2023, Doi: 10.1109/Twc.2022.3226753.
- [9]. S. Khan, B. Ray, And N. Karmakar, "Fingerprinting Chipless Rfid With A Mimo System For Tag Authentication In Internet Of Things," Internet Things, Vol. 31, 2025, Art. No. 101542, Doi: 10.1016/J.Iot.2025.101542.
- [10]. H. Rmili, J. Yousaf, O. Boularess, Et Al., "Enhancing Hajj Pilgrimage Experience And Crowd Management Through Hajj-Related Keywords-Based Chipless Rfid Tags," Alex. Eng. J., Vol. 119, Pp. 56–63, 2025, Doi: 10.1016/J.Aej.2025.01.125.
- [11]. M. Saikat, C. Yihang, C. Mark, A. Ali, G. Mahrnoud Yousef, And C. Premjeet, "Hybrid Rfid-Based Batteryless Seat Sensor With Discontinuous Rf Transmission," Ieee Trans. Veh. Technol., Vol. 71, No. 3, Pp. 2305–2318, 2022, Doi: 10.1109/Tvt.2022.3145431.
- [12]. K. Grishma, R. Biplob, K. Nemai Chandra, And C. Jinho, "Physical-Layer Detection And Security Of Printed Chipless Rfid Tag For Internet Of Things Applications," Ieee Internet Things J., Vol. 9, No. 17, Pp. 15714–15724, 2022, Doi: 10.1109/Jiot.2022.3151364.

- [13]. T. Korfiati, N. C. Vazouras, C. Bolakis, Et Al., "Design, Fabrication And Testing Of A Multifrequency Microstrip Rfid Tag Antenna On Si," Computation, Vol. 12, No. 6, 2024, Art. No. 122, Doi: 10.3390/Computation12060122.
- [14]. C. Bijoy Dripta Barua, M. Sara, S. Young-Jun, K. Chieri, And T. Russell, "A Dynamic Hmm-Based Real-Time Location Tracking System Utilizing Uhf Passive Rfid," Ieee J. Radio Freq. Identif., Vol. 6, Pp. 41–53, 2021, Doi: 10.1109/Jrfid.2021.3102507.
- [15]. Y. Chung And T. H. Berhe, "Long-Range Uhf Rfid Tag For Automotive License Plate," Sensors, Vol. 21, No. 7, 2021, Art. No. 2521, Doi: 10.3390/S21072521.
- [16]. B. Pawłowicz, B. Trybus, M. Salach, Et Al., "Dynamic Rfid Identification In Urban Traffic Management Systems," Sensors, Vol. 20, No. 15, 2020, Art. No. 4170, Doi: 10.3390/S20154170.
- [17]. B. Tara, L. Maisy, C. Weitung, D. Laura, E. Aline, And A. Fadel, "Exploiting Synergies Between Augmented Reality And Rfids For Item Localization And Retrieval," In Proc. Ieee Int. Conf. Rfid (Rfid), 2023, Pp. 30–35, Doi: 10.1109/Rfid58307.2023.10178452.
- [18]. T. T. Tobias, S. Jan, K. Patrick, S. Christian, A. Klaus, And P. Nils, "Expanding The Capabilities Of Automotive Radar For Bicycle Detection With Harmonic Rfid Tags At 79/158 Ghz," Ieee Trans. Microw. Theory Techn., Vol. 71, No. 1, Pp. 320–329, 2023, Doi: 10.1109/Tmtt.2022.3219541.
- [19]. A. T. Mobashsher, A. J. Pretorius, And A. M. Abbosh, "Low-Profile Vertical Polarized Slotted Antenna For On-Road Rfid-Enabled Intelligent Parking," Ieee Trans. Antennas Propag., Vol. 68, No. 1, Pp. 527–532, 2020, Doi: 10.1109/Tap.2019.2939590.
- [20]. J. Yang, Z. Luo, N. Zhang, Et Al., "Numerical Calibration Method For Vehicle Velocity Data From Electronic Registration Identification Of Motor Vehicles Based On Mobile Edge Computing And Particle Swarm Optimization Neural Network," Complexity, 2020, Art. No. 2413564, Doi: 10.1155/2020/2413564.
- [21]. J. Su, A. X. Liu, Z. Sheng, Et Al., "A Partitioning Approach To Rfid Identification," Ieee/Acm Trans. Netw., Vol. 28, No. 5, Pp. 2160–2173, 2020, Doi: 10.1109/Tnet.2020.3004852.
- [22]. T. Lin, C. Hui, Z. Li, And H. Ningjian, "Value-Driven Uncertainty-Aware Data Processing For An Rfid-Enabled Mixed-Model Assembly Line," Int. J. Prod. Econ., Vol. 165, Pp. 273–281, 2015, Doi: 10.1016/J.Ijpe.2014.12.030.
- [23]. Prairie View A & M Univ., Civil And Mechanical Engineering Technology, Et Al., "An Investigation Of Factors Influencing Performance Of Rfid: Applications In Transportation," J. Transp. Lit., Vol. 10, No. 4, Pp. 49–53, 2016, Doi: 10.1590/2238-1031.Jtl.V10n4a5.
- [24]. A. Ganjar, S. Muhammad, F. Umar, M. R. Muhammad, M. A. S., N. L. F., J. Lee, And J. Ryu, "Improving Efficiency Of Rfid-Based Traceability System For Perishable Food By Utilizing Iot Sensors And Machine Learning Model," Food Control, Vol. 110, 2020, Art. No. 107016, Doi: 10.1016/J.Foodcont.2019.107016.
- [25]. Y. I. Yang, W. S. Yu, W. J. Park, Et Al., "Development Of Accelerated Life Test Method For Uhf Rfid Tags For Medicine Supply Management," J. Appl. Reliab., Vol. 14, No. 2, Pp. 93–96, 2014.
- [26]. A. Bernard, X. Wang, J. Zhang, S. Ma, P. Senthilkumar C. G., And J. P., "Optimizing Adaptive Power Control For Enhancing Robustness In Rfid Sensing," In Proc. Ieee Int. Conf. Rfid-Technol. Appl. (Rfid-Ta), 2024, Pp. 157–160, Doi: 10.1109/Rfid-Ta64374.2024.10965152.
- [27]. W. Dirk, B. Dennis, R. Carmen, S. Bernd, And F. Michael, "Towards A Standardised Information Exchange Within Finished Vehicle Logistics Based On Rfid And Epcis," Int. J. Prod. Res., Vol. 55, No. 14, Pp. 4136–4152, 2016, Doi: 10.1080/00207543.2016.1254354.